A Journal of the Gesellschaft Deutscher Chemiker

Angewandte International Edition GDCh Chemie

www.angewandte.org

Accepted Article

Title: Cationic Micelle as An In Vivo Catalyst for Tumor-Localized Cleavage Chemistry

Authors: Chunhong Wang, Hanyu Hong, Mengqi Chen, Zexuan Ding, Yuchen Rui, Jianyuan Qi, Zi-Chen Li, and Zhibo Liu

To be cited as: *Angew. Chem. Int. Ed.* 10.1002/anie.202106526

Link to VoR: https://doi.org/10.1002/anie.202106526

WILEY-VCH

10.1002/anie.202106526

WILEY-VCH

RESEARCH ARTICLE

Cationic Micelle as An *In Vivo* Catalyst for Tumor-Localized Cleavage Chemistry

Chunhong Wang,[a] Hanyu Hong, [a] Mengqi Chen, [a] Zexuan Ding, [a] Yuchen Rui, [a] Jianyuan Qi, [a] Zi-Chen Li, [c] Zhibo Liu*[a,b]

Abstract: The emerging strategies of accelerating the cleavage reaction in tumor through locally enriching the reactants is promising. Yet, the applications are limited due to the lack of the tumor-selectivity for most of the reactants. Here we explored an alternative approach to leverage the rate constant by locally inducing an *in vivo* catalyst. We found that the desilylation-induced cleavage chemistry could be catalyzed *in vivo* by cationic micelles, and accelerated over 1400-fold under physiological condition. This micelle-catalyzed controlled release platform is demonstrated by the release of a 6-hydroxyl-quinoline-2-benzothiazole derivative (HQB) in two cancer cell lines and a NIR dye in mouse tumor xenografts. Through intravenous injection of a pH-sensitive polymer micelles, we successfully applied this strategy to a prodrug activation of hydroxyl camptothecin (OH-CPT) in tumors. Its "decaging" efficiency is 42-fold to that without cationic micelles–mediated catalysis. This micelle-catalyzed desilylation strategy unveils the potential that micelle may act beyond a carrier but a catalyst for local perturbing or activation.

Tuning the reaction rate in a tissue-selective manner is highly demanding for both biomedical research and clinical usage, yet is still an unmet challenge. [1] In the lab, a chemist could adjust the reaction rate by changing the temperature, reaction medium, substrate concentration or adding catalyst and etc.[2] Nevertheless, the strategies that could control the reaction rate *in vivo* are limited, let alone in a tissue-selective manner. Most of the bioorthogonal cleavage chemistries[3] involve two reaction components, a "caged" functional molecule and a "decaging" reagent[4], therefore their reaction rates often conform to the law of the second-order reaction. Recently, strategies that could co-locally enrich two reaction components in the tissue or organelle of interest (e.g. tumor[5] or mitochondrion[1c]) have been established, allowing to leverage the reaction rate in a tumor-selective manner. However, these strategies depend on the tumor-selectivity of the two reactants, that have limited their applications. Here we explored the idea of whether the reaction rate could be leveraged by locally manipulating the rate constant, which would be feasible to catalyze many bioorthogonal reactions *in vivo.*

Micelles or liposomes have been widely used in the deliveries of small molecule drugs[6], nucleic acids[7], bacterial effectors[8] and proteins[9]. These nano-carriers could be featured with tissue-selectivity by tuning up their compositions[10] or decorating receptor-based targets[11]. Interestingly, micelle has also been widely used in accelerating a couple of organic reactions in water[12], which often face the loss of reactivity when induced into the water phase from the organic solvent. It is a combinational effect synergizing from hydrophobic effect, enrichment effect and solvent effect[13]. If the local rate constant of a bioorthogonal cleavage chemistry could be increased by a tumor-enriched micelle, it would provide an ideal means to release the "client" molecule or rescue the function of protein in a tumor-selective manner.

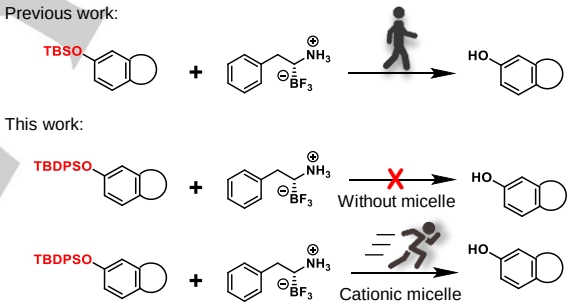

Scheme 1. Micelle-catalyzed Phe-BF_3-mediated desilylation enabled controlled release of functional molecules and is remarkably faster than that without micellar catalysis.

Recently, we established a novel bioorthogonal chemistry, in which a cell-enterable amino acid mimetic Phe-BF_3 [14] specifically and efficiently desilylates and "cleaves" an optimized silyl ether-containing carbamate linker, which enables tumor-selective activation of gasdermin and then triggers potent T cell-mediated antitumor immunity[5]. Here we are pleased to offer a more advanced strategy that utilizing micellar catalysis to manipulate the local rate constant to control the bioorthogonal cleavage chemistry in the tumor. Under physiological conditions, TBDPS (*tert*-Butyldiphenylsilyl) is generally the most robust silyl ether protecting group towards fluoride-mediated desilylation.[15] The desilylation rate constant of TBDPS is about 1/1,000,000 that of de-protecting TMS and 1/100 that of de-protecting TBS, respectively. Herein, we choose Phe-BF_3-mediated TBDPS deprotection as a proof of concept to study the catalytic efficacy of micelle in test tubes, living cells and tumor-bearing mice. We found that micelle-catalyzed desilylation is highly efficient (**Scheme 1**). Without micellar catalysis, desilylation of a TBDPS-

[a] C. H. Wang, H. Y. Hong, M. Q. Chen, Dr. Z. X. Ding, Y. C. Rui, J. Y. Qi, Prof. Dr. Z. B. Liu
College of Chemistry and Molecular Engineering, Peking University, Beijing, 100871 (China)
Radiation Chemistry Key Laboratory of Fundamental Science, Beijing National Laboratory for Molecular Sciences, E-mail: zbliu@pku.edu.cn.
[b] Prof. Dr. Z. B. Liu
Peking University-Tsinghua University Center for Life Sciences, Beijing, 100871 (China)
[c] Prof. Dr. Z. C. Li,
Beijing National Laboratory for Molecular Sciences, Key Laboratory of Polymer Chemistry & Physics of Ministry of Education, Department of Polymer Science & Engineering, College of Chemistry and Molecular Engineering, Center for Soft Matter Science and Engineering, Peking University
Beijing 100871 (China)

Supporting information for this article is given via a link at the end of the document.

10.1002/anie.202106526

protecting molecule hardly occur with 10 mM Phe-BF_3 in 12 hours, but readily finishes in 30 min when treated with cationic micelles+10 mM Phe-BF_3 (**Scheme 1** and **Figure S1**). Besides, in the aspect of prodrug design, the more stable the "caging" group, the less off-target release it would cause to normal tissues.[16] Thus, we expect that micellar catalysis–activated prodrug, especially caged by TBDPS, would exhibit less side-effect and more selectivity for tumor-targeting drug release.

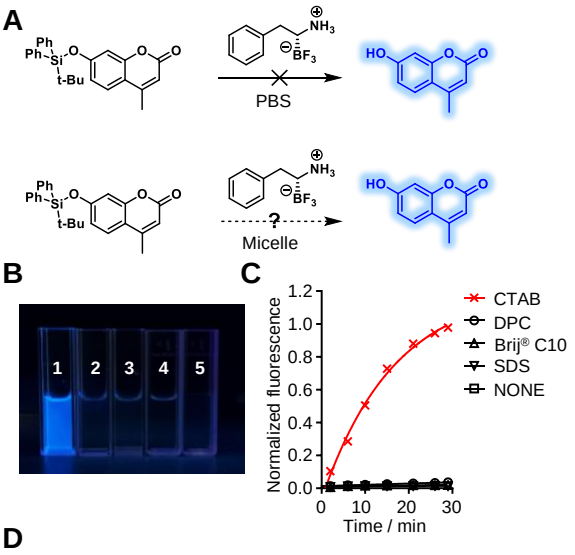

D

Rate constants of Phe-BF_3-mediated desilylation

Types	CTAB	DPC	Brij® C10	SDS	NONE
k / $M^{-1}.s^{-1}$	3.13 ± 0.31	0.027 ± 0.001	0.014 ± 0.003	0.0048 ± 0.0023	0.0021 ± 0.0002
k / k_{NONE}	1490 ± 150	12.8 ± 0.5	6.67 ± 1.42	2.28 ± 1.09	1.00

Figure 1. A cationic CTAB micelle was identified as the catalyst that can accelerate Phe-BF_3-mediated desilylation by >1000-fold. (A) Schematic representation of micelle-catalyzed desilylation releases coumarin from TBDPSO-Coumarin. (B) Photographs showing the fluorescence from TBDPSO-Coumarin samples treated with 0.50 mM Phe-BF_3 and cationic CTAB micelle (1), zwitterionic DPC micelle (2), neutral Brij® C10 micelle (3), anionic SDS micelle (4) and no surfactant (5), respectively. The concentrations of the surfactants 1-3 and 4 are 2.0 mM and 10.0 mM, respectively. And, the reaction time is 10 min. (C) Fluorescence-time curve of TBDPSO-Coumarin treated by 0.50 mM Phe-BF_3 and the indicated micelles (2 mM or 10 mM surfactants in PBS, pH=7.4) (D) Rate constants summary of micelle-catalyzed Phe-BF_3-mediated desilylation.

To explore this micelle-catalyzed desilylation strategy, we firstly constructed a TBDPS-"caged" coumarin, in which the TBDPS group is directly linked to the electron-donating phenolic oxygen (**Figure 1A**). Free coumarin, as opposed to the oxygen-blocked coumarin in the silyl-phenolic ether system, is highly fluorescent, thus providing a simple and quantitative assay for micelle-catalyzed desilylation. Phe-BF_3-mediated desilylation follows a mechanism that involves no free fluoride intermediate, and the fluoride is transferred directly from the trifluoroborate to the empty d-orbital of the silicon atom on the silyl ether. Therefore, an environment that could stabilize the fluoride-transfer transition state, cationic micelle might be preferred, would decrease the activation energy and accelerate the desilylation.

As reported previously, the net charge of micelle surfactant often greatly impacts the efficacy of micellar catalysis. The paired micelle and reactant are often counter-charged: anionic surfactant micelles often accelerate metal cation–mediated coupling reaction[17] and cationic micelles often catalyze the fluoride-mediated desilylation[18]. Though trifluoroborate (-BF_3) is negatively charged, Phe-BF_3 is neutral. To find the "perfect match" that could catalyze Phe-BF_3-mediated desilylation, we screened four micelles formed by the surfactants with different net charges, including cationic CTAB (Cetyltrimethylammonium bromide), anionic SDS (Sodium dodecyl sulfate), zwitterionic DPC (Dodecylphosphocholine) and nonionic Brij® C10 (Polyoxyethylene (10) cetyl ether). To ensure micelle formation, the concentration of these surfactants in phosphate buffer saline (PBS) is 2 mM or 10 mM, which is higher than their corresponding critical micelle concentrations (CMC).[13, 19], The stability of TBDPSO-coumarin was evaluated in the above micelles prior to treated by Phe-BF_3 (**Figure S2**, dotted curve), indicating that the reaction was triggered by Phe-BF_3 not the micelle itself. As shown in **Figure 1B**, intense fluorescence was detected within 10 min after treating TBDPS-coumarin+Phe-BF_3 with cationic CTAB micelle. Meanwhile, almost no fluorescence was observed from other samples that were treated with anionic SDS micelle, zwitterionic DPC micelle, and non-ionic Brij® C10 micelles or without micelle in PBS. More quantitatively, the kinetic profiles of micelle-catalyzed desilylation were further investigated according to the fluorescence increase (**Figure 1C**). The curves fit well with the second-order reaction and the rate constants are summarized in **Figure 1D**. The second-order rate constant of Phe-BF_3-desilylation in cationic CTAB micelle is 3.13 ± 0.31 $M^{-1}.s^{-1}$, which is over 3-magnitude larger than that without micellar catalysis (i.e. 0.0021 ± 0.0002 $M^{-1}.s^{-1}$). The rate constants in anionic SDS micelle, non-ionic Brij® C10 micelle and zwitterionic DPC micelle are 0.0048 ± 0.0023 $M^{-1}.s^{-1}$, 0.014 ± 0.003 $M^{-1}.s^{-1}$ and 0.027 ± 0.001 $M^{-1}.s^{-1}$, respectively. These values are 2-12 folds larger than that of micelle free systems, yet are much smaller than that of cationic micelle–catalyzed system. As summarized in the bottom line of **Figure 1D**, if the rate constant without micellar-catalysis is standardized as 1.00, the catalytic efficacy of cationic, zwitterionic, non-ionic and anionic micelles would be 1490 ± 150, 12.8 ± 0.5, 6.67 ± 1.42 and 2.28 ± 1.09, respectively. This result corroborates with our hypothesis that cationic micelle might be the perfect match to catalyze Phe-BF_3-mediated desilylation.

The stability of the "caging" group is another key issue in developing the cleavage chemistry needed for in vivo manipulation.[20] In general, a stable "caged" molecule should remain >90% in 24 hours.[5] In the above study, we found that though TBDPSO-coumarin is stable in PBS (**Figure S1**), its stability in CTAB is insufficient (**Figure S2**). Then, we screened various TBDPS-protected phenols to study the structure-stability relationship. As shown in **Figure 2A**, the substitutions of these compounds include strong electron-withdrawing groups (compound **1-4**), mild or weak electron-withdrawing groups (compound **5-13**), no substitution (compound **14**), and electron-donating groups (compound **15).** The relationship between a given substituent and its effect on the pKa of a phenol represents one of the fundamental correlations in physical organic chemistry. We wondered if the hydrolytic stability of TBDPS-protected phenol was related to its pKa value. If so, knowledge of the pKa of a given phenol can be used to rationally design TBDPS-protected phenol with predictable stability.

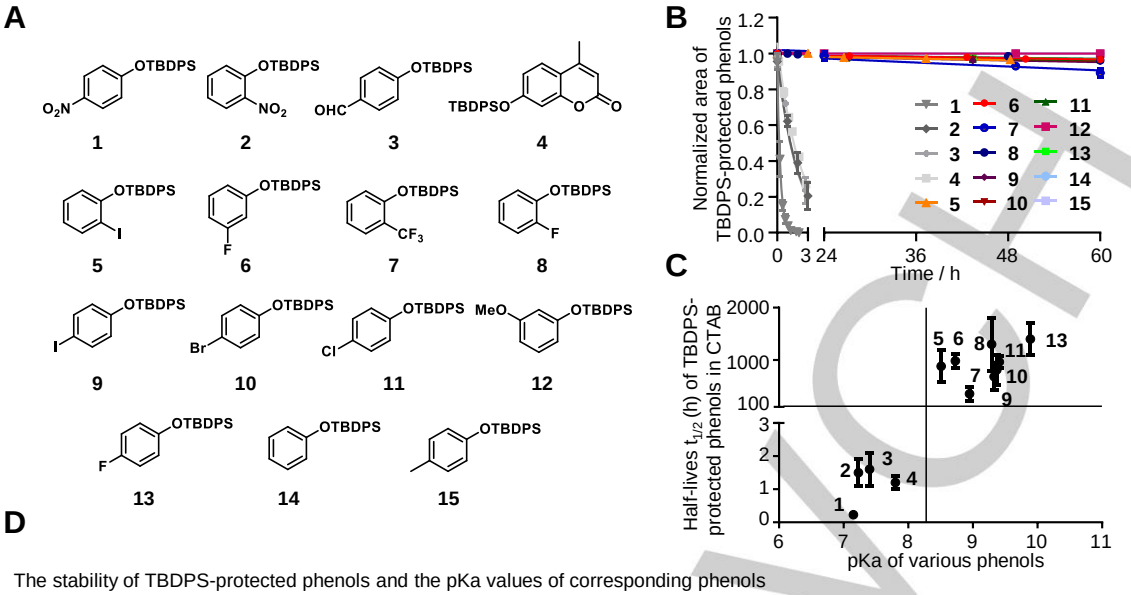

D

The stability of TBDPS-protected phenols and the pKa values of corresponding phenols

No.	pKa	k_w (h^{-1})	$t_{1/2}$ (h)	No.	pKa	k_w (h^{-1})	$t_{1/2}$ (h)	No.	pKa	k_w (h^{-1})	$t_{1/2}$ (h)
1	7.15	3.1 ± 0.2	0.23 ± 0.03	**6**	8.73	(7.1 ± 0.4) ×10^{-4}	(9.8 ± 1.4) ×10^{2}	**11**	9.41	(7.2 ± 0.5) ×10^{-4}	(9.6 ± 1.2) ×10^{2}
2	7.23	0.45 ± 0.05	1.5 ± 0.4	**7**	8.95	(2.5 ± 0.4) ×10^{-3}	(3.5 ± 1.4) ×10^{2}	**12**	9.65	n.d.	n.d.
3	7.4	0.42 ± 0.05	1.6 ± 0.5	**8**	9.29	(5.1 ± 0.4) ×10^{-4}	(1.3 ± 0.5) ×10^{3}	**13**	9.89	(4.9 ± 0.4) ×10^{-4}	(1.4 ± 0.3) ×10^{3}
4	7.8	0.58 ± 0.05	1.2 ± 0.2	**9**	9.33	(1.0 ± 0.1) ×10^{-3}	(6.8 ± 2.6) ×10^{2}	**14**	9.99	n.d.	n.d.
5	8.51	(7.9 ± 0.8) ×10^{-4}	(8.8 ± 3.1) ×10^{2}	**10**	9.37	(8.5 ± 1.0) ×10^{-4}	(8.1 ± 2.9) ×10^{2}	**15**	10.26	n.d.	n.d.

Figure 2. A structure-stability relationship study of TBDPS-protected phenols in CTAB. (A) Chemical structures of TBDPS-protected phenols with different substituents. (B) Time-stability curves of compound **1-15** in CTAB solution. (C) A correlation-analysis about the half-lives of TBDPS-protected phenols in CTAB and the pKa values of the corresponding phenols. (D) Data summary. The pKa values were referred to "CRC Handbook of Chemistry and Physics, the 91st Edition" [21]. The general experimental condition is 0.10 mM of substrates in PBS of 2mM CTAB solution. n.d., not detected.

A systematic kinetic study was performed to investigate their hydrolytic stabilities. The hydrolysis curve follows a pseudo first-order reaction (**Figure 2B)**. The half-lives and kinetic constants of TBDPS-protected phenols and the pKa values of their corresponding phenols are summarized in **Figure 2D**. If a molecule remains more than 90% after 24 hours, it means that the corresponding half-life should be over 170 hours. The half-lives of compound **1-4** in CTAB are 0.23 ± 0.03 h, 1.5 ± 0.4 h, 1.6 ± 0.5 h, 1.2 ± 0.2 h, respectively (**Figure 2B** and **Figure 2D**). They cannot afford the stability required for the *in vivo* cleavage chemistry. To our satisfaction, the hydrolysis rates of rest compounds are remarkably slower (**Figure 2B**). The half-lives of compound **5-15** are above 300 hours, and hydrolytic products of **12**, **14**, and **15** are almost negligible (**Figure 2D**). Interestingly, the pKa values of corresponding phenols of compounds **1-4** are below 8, while the rest are above 8.5 (**Figure 2C**). Therefore, we conclude that a TBDPS-protected phenol should be stable enough for micelle-catalyzed desilylation when its corresponding pKa is >8.5.

Hydroxyquinoline is an important pharmaceutical synthon and has been the core structure for a couple of FDA-approved anti-cancer drugs, including Topotecan, Oxyquinoline, Chloroxine, Tilbroquinol, etc. In addition, the pKa of 6-hydroxyquinoline is about 8.8. To further expand the substrate scope of this micelle-catalyzed desilylation, we replaced the model compound with the TBDPS-"caged" hydroxyquinoline derivatives. As presented in **Figure 3A**, TBDPSO-HQB was synthesized as a fluorogenic probe to monitor the progress of the desilylation.[22] Meanwhile, to expand the strategy to living systems, we should solve the problem of the bioorthogonality and the biocompatible catalytic efficiency of the micellar catalytic reaction. We firstly assayed the bioorthogonality of micelle-catalyzed desilylation by treating TBDPSO-HQB (2 μM) with various biologically relevant molecules at 37 °C in 2 mM CTAB PBS solution. No false-positive fluorophore response was observed at 2 hours in the absence of Phe-BF_3 and these will not affect the decaging reaction induced by Phe-BF_3 (**Figure 3B**). The impacts on catalytic efficacy from counter anions of micelles are presented as in **Figure 3C**, and no significant difference has been observed. Interestingly, as shown in **Figure3D**, we find that the chain length of surfactant has great impact on catalytic efficiency. The desilylation rate constant in 2mM dodecyl trimethylammonium bromide (DTAB, C12) dropped to 0.06 ± 0.012 $M^{-1}\cdot s^{-1}$, which is only half of that in 2 mM tetradecyl trimethyl ammonium bromide (TTAB, C14). Almost no fluorophore has been detected in octyl trimethylammonium bromide (OTAB, C8) or butyl trimethylammonium bromide (BTAB, C4). It is known that the CMC values are often chain length–dependent. The CMC values of DTAB, OTAB and BTAB in PBS are 20 mM, 600 mM and above 1.0 M, respectively, which are 1-3 magnitudes over that of CTAB (**Figure S5**). The above data suggests that freely dissolved cationic unimers would not catalyze this desilylation-mediated approach. In addition, we have also tried to use polyethyleneimine (PEI) to catalyze the decaging reaction. Though it carries more positive charges, no released

10.1002/anie.202106526

fluorescence was observed (**Figure S6**). In conclusion, we would suggest that disassembled cationic unimers can not catalyze Phe-BF_3-mediated desilylation, and their abilities to form the intact micelles are critical for catalytic efficiency.

We then wondered whether micelle-catalyzed desilylation could be developed into a useful controlled release system, making micelle as a nano-enzyme for *in vivo* catalysis. Unfortunately, the progress of pursuing this idea has been postponed by the unacceptable cytotoxicity of CTAC. As shown in **Figure 3E** and **Figure S7**, the cell viability of 12 μM CTAC is below 20 % for both BGC823 and U87. But its catalytic efficiency dropped sharply when its concentration is below 100 μM (grey bar, **Figure 3F**). No reaction occurred in 4 hours when the Phe-BF_3-mediated desilylation is incubated with 12 μM or 25 μM CTAC (grey bar, **Figure 3F**). Therefore, though working well *in vitro*, CTAC micelle could not catalyze desilylation *in vivo*. To discover a cationic surfactant with low cytotoxicity and low CMC, we have evaluated two alternative candidates: dihexadecyl dimethylammonium chloride (DHAC) and 1,2-dioleoyl-3-trimethylammonium-propane chloride (DOTAP), by the same set of assays. As shown in **Figure 3E** and **3F**, DOTAP micelle shows better biocompatibility and higher catalytic efficiency to Phe-BF_3-mediated desilylation than both DHAC and CTAC. In addition, it has been widely used for gene/nucleic acid delivery in preclinical studies and clinics[7], so DOTAP micelle was chosen as the catalyst to accelerate the Phe-BF_3-mediated desilylation in living cells and tumor-bearing mice.

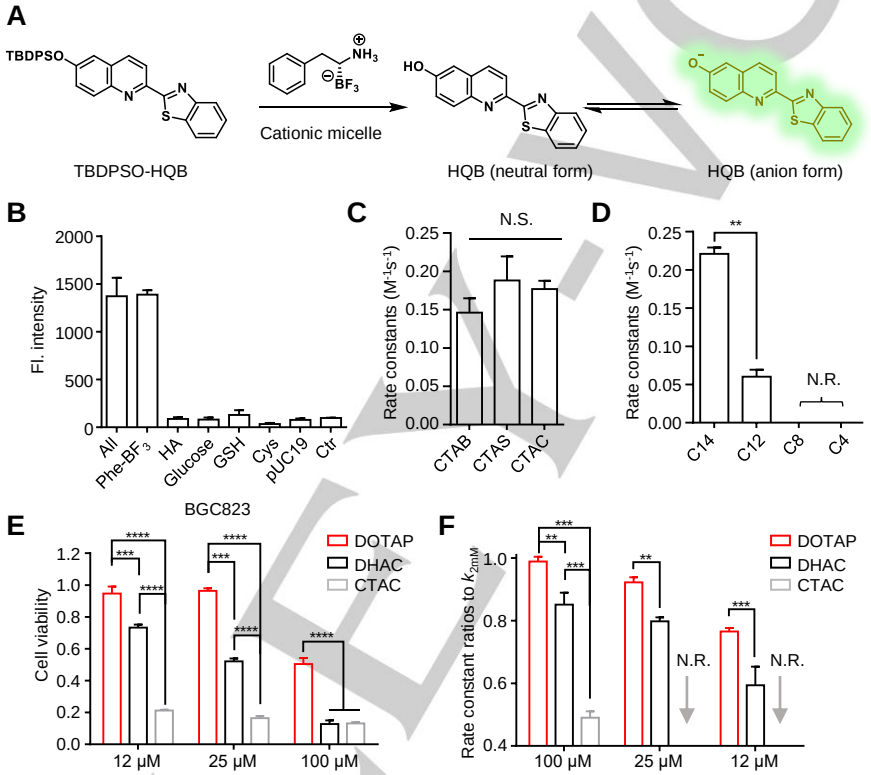

Figure 3. Optimization of the cationic micelles for better biocompatibility and higher catalytic efficiency to Phe-BF_3-mediated desilylation. (A) Schematic representation of Phe-BF_3-induced desilylation that can release the fluorescence-"caged" 6-hydroxyl-quinoline-2-benzothiazole (HQB). (B) Fluorescence-emission assay of possible desilylation of TBDPSO-HQB (2 μM) by various biologically relevant molecules (2 mM for Phe-BF_3, Glucose, GSH, Cys; 0.5 mg/ml for HA, hyaluronic acid, 4k; 1 ng/L for plasmid pUC19; and 'All' means the combination of above reagents). The HQB fluorescence intensity was determined at 37°C in 2 mM CTAB phosphate buffered solution with λ_{ex} = 360 nm and λ_{em} = 535 nm (n = 3). (C) Rate constant analysis of micelle-catalyzed desilylation treated by 2 mM cyltrimethylammonium with bromide (CTAB), sulfonate (CTAS) and chloride (CTAC) as the counter anions (n = 3). (D) Rate constant analysis of micelle-catalyzed desilylation treated by 2 mM alkyl trimethylammonium bromide with different side chain length (n = 4). (E) Cytotoxicity of 12 μM, 25 μM and 100 μM of DOTAP, DHAC and CTAC against BGC823 cells, respectively (n = 3). (F) The rate constant ratios of Phe-BF_3-mediated desilylation catalyzed by 100 μM, 25 μM and 12 μM of indicating surfactants to 2mM of the micelles, respectively. N.S., no significant difference, N.R. no reaction. Data are shown as mean ± s.d.; two-tailed unpaired Student's *t*-test was performed (***P* < 0.01, ****P* < 0.001, *****P* < 0.0001). The above assays were performed at 37 ℃ without further notification.

To test whether micellar catalysis works in living cells, we pre-treated BGC823 and U87 cancer cells with 20 μM TBDPSO-HQB or HQB. The cells were rinsed with PBS after incubation for 2 hours, followed by treatment with 40 μM DOTAP and 200 μM Phe-BF_3. The cell viability of two cell lines with 40 μM DOTAP, was evaluated prior to the kinetics study, and no obvious cytotoxicity has been observed (**Figure S7**). In addition, TBDPSO-HQB and Phe-BF_3 have also been tested, and show no toxic to the two cells (**Figure S8**). As illustrated in **Figure 4A**, the combinational treatment of the TBDPSO-HQB+Phe-BF_3+DOTAP successfully release the "caged" fluorophore and highlight the cells, while almost no fluorescence was captured in the groups treated with TBDPSO-HQB+DOTAP, TBDPSO-HQB+Phe-BF_3 and TBDPSO-HQB only. After subtracting the cell auto-fluorescence background, the fluorescence intensity of the TBDPS-HQB+Phe-BF_3+DOTAP group is a 5.8-fold increase in BGC823 cells (**Figure 4B**) and a 4.4-fold increase in U87 cells (**Figure 4C**) compared to the control groups, respectively. This result indicates that DOTAP micelle could catalyze Phe-BF_3-mediated desilylation in living cells.

We then examined whether micellar catalysis could trigger desilylation of TBDPS-caged functional molecule and liberate the

client fluorophore in tumor-bearing mice. We prepared a TBDPS-"caged" near-infrared dye (**Figure 5A**), denoted as TBDPSO-NIR, to sense the desilylation-to-release with optical imaging in tumor-bearing mice.[23] TBDPSO-NIR is highly stable and showed no spontaneous desilylation even after 12-h incubation in PBS (**Figure S9**). We performed a head-to-head comparison on the dual-tumor-bearing mice. For mouse #1 in **Figure 5B**, as the negative-control group, its left tumor and right tumor were intratumorally injected with TBDPSO-NIR and TBDPSO-NIR+DOTAP, respectively. No fluorescence release was observed in both tumors. For mouse #2, its left tumor and right tumor were intratumorally injected with TBDPSO-NIR and TBDPSO-NIR+DOTAP, respectively, followed tail-vein injection of Phe-BF_3. As expected, intense fluorescence was observed on the right tumor at 5 hours after the injection of Phe-BF_3, while there is no fluorescence on the left tumor. For mouse #3, as the positive-control group, its left tumor and right tumor were intratumorally injected with TBDPSO-NIR and OH-NIR+DOTAP, respectively. No fluorescence is on the left tumor and the fluorescence on the right tumor is relatively as strong as the right tumor of mouse #2. The fluorescence intensities were analyzed and summarized as in **Figure 5C**. After subtracting the autofluorescence background, the fluorescence intensity of the tumor sequentially treated with TBDPSO-NIR+DOTAP and followed by Phe-BF_3 is nearly as strong as the positive control tumor, and is significantly higher than the tumors treated without Phe-BF_3 or micelle. This result corroborates with the optical imaging studies, and suggests that TBDPS-"caged" molecules are stable *in vivo* and DOTAP micelle could catalyze Phe-BF_3-mediated desilylation in tumor-bearing mice.

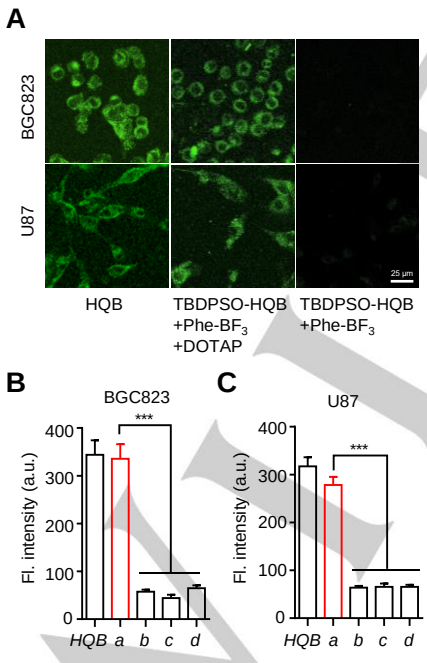

Figure 4. Micelle-catalyzed desilylation can release the "caged" fluorescent HQB from the robust TBDPSO-linker in living cells. (A) Representative confocal fluorescence images (40x fold) of BGC823 and U87 cells. The cells were pretreated with HQB or TBDPS-HQB (20 μM in RPMI-1640) for 2 hours and washed twice with PBS, followed by incubating with DOTAP (40 μM), Phe-BF_3 (200 μM) and DOTAP (40 μM)+Phe-BF_3 (200 μM), respectively. (B, C) Fluorescence intensity analysis in BGC823 (B) or U87 (C) cells according to the examined field of view by confocal microscopy. The cells were treated with HQB, TBDPSO-HQB+Phe-BF_3+DOTAP (a), TBDPSO-HQB+DOTAP (b), TBDPSO-HQB+Phe-BF_3 (c) and TBDPSO-HQB only (d), respectively. Twenty fields of view were randomly chosen for each experiment (two-tailed unpaired Student's t-test, ***P < 0.001).

Encouraged by the success of the micelle-catalyzed desilylation that efficiently releases the fluorophores *in vitro* and *in vivo*, we were confident that a broader substrate scope will work as well with this micellar catalysis–induced release strategy. Here, we used 10-hydroxycamptothecin (OH-CPT) as a model anticancer molecule to invent a prodrug by taking the aforementioned catalysis-to-release strategy. The prodrug was denoted as TBDPSO-CPT, and its release process is shown in **Figure 5D**. The cytotoxicity of TBDPSO-CPT, OH-CPT and catalysis-activated HO-CPT was assayed in U87 (**Figure S10A**), BGC823 (**Figure S10B**), MC38 (**Figure S10C**) and CHO (**Figure S10D**) cell lines, respectively. In most cases, the cell viabilities of TBDPSO-CPT are much better than HO-CPT to the four cell lines. The cell viability curves of cells treated by TBDPSO-CPT+DOTAP or TBDPSO-CPT+Phe-BF_3 are not remarkably different from the curves of TBDPSO-CPT (**Figure S10**). The cell viability curves of catalysis-activated HO-CPT almost coincide with the curve of OH-CPT, indicating the effectiveness of micelle-catalyzed release. The IC50 of OH-CPT against BGC823 cells is 1.27 ± 0.17 μM and the IC50 of TBDPSO-CPT against BGC823 cells is 22.08 ± 6.12 μM, which is 17-fold over its parent drug. The IC50 of activated OH-CPT against BGC823 cells is 1.66 ± 0.16 μM, which is about the same as the IC50 of OH-CPT. The IC50s of TBDPSO-CPT, OH-CPT and catalysis-activated HO-CPT against other cell lines are listed in **Figure S11**, which are corroborative with the cell viability curves.

To accomplish micelle-catalyzed desilylation triggered drug release in the tumor, a sustainable tumor accumulation of micelle is essential. The retention and local concentration of DOTAP in the tumor were investigated by positron emission tomography (PET)[24]. As shown in **Figure S12A** most of the intratumorally injected ^{89}Zr-labelled DOTAP-micelle (200 μM, 20 μL PBS) stayed in the tumor within 24 hours, while almost no uptake was observed in other tissues. According to the 3-dimensional quantitative analysis of the radioactive signals in the region-of-interest (ROI), over 90% of [^{89}Zr] DOTAP-micelle remained in the tumor at 24 hours post-injection (**Figure S12B**), corroborating with the dominated tumor uptake in PET imaging. As the tumor volumes are 30-40 mm^3 at the moment, the local concentration of DOTAP is up to 100 μM, which should be high enough to form stable micelles and catalyze the desilylation (**Figure S5B**). Besides, the long tumor retention of DOTAP also indicates that micelles have been formed in tumor, otherwise DOTAP would clear from tumor much faster as a small molecule.[25]

The treatment efficacy of this prodrug activation system was evaluated on BGC823 tumor-bearing mice (**Figure 5E**). DOTAP (200 μM, 20 μL PBS) was intratumorally injected prior to the combinational tail-vein injection of TBDPSO-CPT and Phe-BF_3. For the group of mice treated by PBS, the volume of BGC823 tumors increased by > 30-fold in three weeks (**Figure 5F**). For the group treated by TBDPSO-CPT only, TBDPSO-CPT+Phe-BF_3 and TBDPSO-CPT+DOTAP, the tumor volume increased by 14.9-fold, 19.4-fold and 16.2-fold, respectively (**Figure 5F**), showing partial yet insufficient treatment efficacy. Upon the treatment with TBDPSO-CPT+Phe-BF_3+DOTAP, remarkable suppressions on tumor growth have been observed (**Figure 5F**, red curve), indicating that the micellar catalysis–triggered prodrug activation is effective in the tumor. The tumors were dissected and then weighed, which further confirmed the antitumor effect of

10.1002/anie.202106526

micellar catalysis strategy (**Figure 5G** and **Figure S12**). Importantly, mice after the treatment do not show significant changes in mice body weight (**Figure S14**). And almost no tissue damage was observed in major organs according to histology analysis (**Figure S15**). However, we found that the uncaged drug OH-CPT shows severe systemic toxicity (**Figure S16**), thus the related tumor growth curve is not included. Collectively, these data suggested the promising potential of the *in vivo* micellar catalysis–induced desilylation with good biological safety.

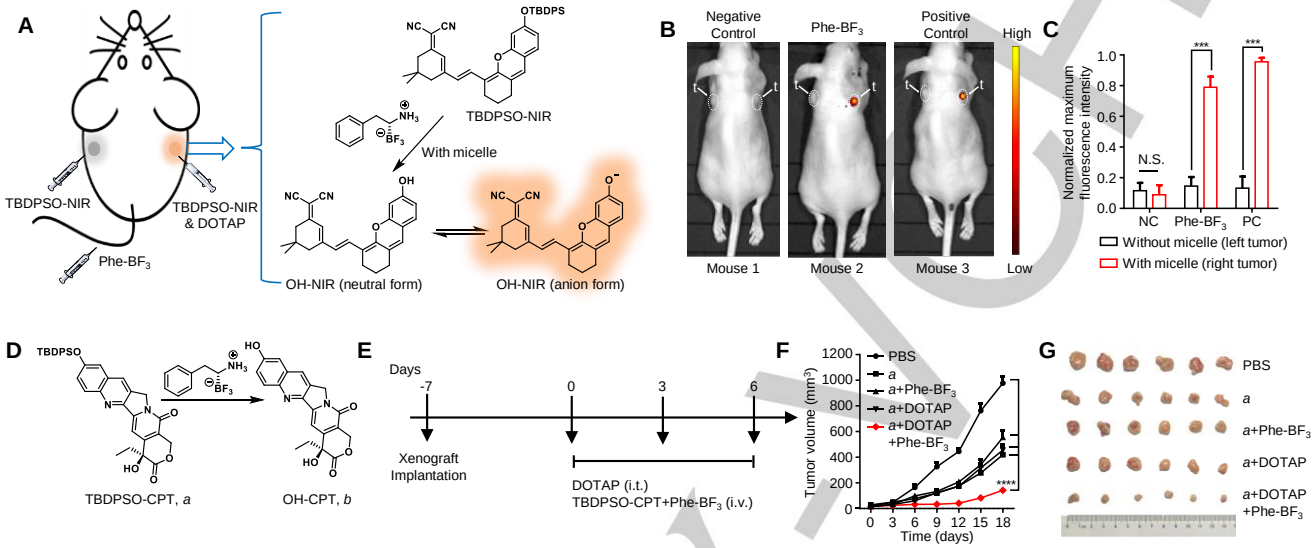

Figure 5. Micelle-catalyzed desilylation can release the "caged" near-infrared fluorescent OH-NIR and hydroxyl camptothecin (OH-CPT) that suppressed tumor growth in mice. (A) Schematic representation of micelle-catalyzed desilylation induced fluorescence release in the right tumors in mice. (B) Representative optical imaging of the tumor-bearing mice. For the left mice, its left tumor and right tumor was intratumorally injected with TBDPSO-NIR and TBDPSO-NIR+DOTAP, respectively. For the middle mice, its left tumor and right tumor was intratumorally injected with TBDPSO-NIR and TBDPSO-NIR+DOTAP, respectively, followed tail-vein injection of Phe-BF_3. For the right mice, its left tumor and right tumor was intratumorally injected with TBDPSO-NIR and OH-NIR+DOTAP, respectively. (C) Comparison of normalized maximum fluorescence intensity of tumors (n = 3, two-tailed unpaired Student's t-test, ***P < 0.001). Optical imaging was taken five hours after treatment. (N.S. no significant difference, NC: negative control, PC: positive control) (D) Scheme of OH-CPT release induced by Phe-BF_3 triggered desilylation. (E) Flow chart of treatment. (F, G) The tumor-bearing mice were intratumorally injected with DOTAP or intravenously injected (i.v.) with PBS, TBDPSO-CPT or Phe-BF_3 alone or in combination. (F) Average tumor volumes of each group of mice. (G) Photograph of the BGC823 tumors on day 18 after treatment.

Since traditional cationic micelles normally clear overly fast from blood circulation, they have difficulties reaching tumors through intravenous injection.[26] To overcome this challenge, we constructed a pH-sensitive PEO_{45}-*b*-$PC7A_5$-*b*-PBA_{25} (PC7BA, **Figure 6A**) micelles as the nano-carriers to further investigate the *in vivo* application of cationic micelles–catalyzed desilylation. As shown in **Figure 6B** and **6C**, PC7BA micelles are neutral to mildly negative-charged at pH = 7.4, and can readily shift to positively charged at pH = 6.5 (acidic tumor microenvironment[27]). The CMC values of PC7BA in PBS buffer are 6.6 μg/mL (pH = 7.4) and 10 μg/mL (pH = 6.5), respectively (**Figure S17**). The hydrodynamic diameters are 15 nm and 45 nm at pH = 6.5 and at pH = 7.4 (**Figure S18**), respectively, which corroborated the observations under the transmission electron microscope (TEM, **Figure S19**). These results suggest that PC7BA micelles can be readily switched into positively charged while keeping intact, which are essential for *in vivo* catalysis.

We have studied their pharmacokinetics by positron emission tomography (**Figure 6D**) and time-activity curve (**Figure 6E**) of ^{89}Zr-labelled PC7BA micelles. As expected, they gave good blood circulation and notable tumor uptake through intravenous injection. Besides, a comparison experiment shows that PC7BA micelles can effectively catalyze the Phe-BF_3-mediated desilylation at pH = 6.5 (**Figure 6F**). Its "decaging" efficiency is 42-fold to that of PLGA-PEG micelles in tumors in mice (**Figure 6G**). The above results suggest that cationic micelles play an important role in accelerating desilylation both *in vitro* and *in vivo*.

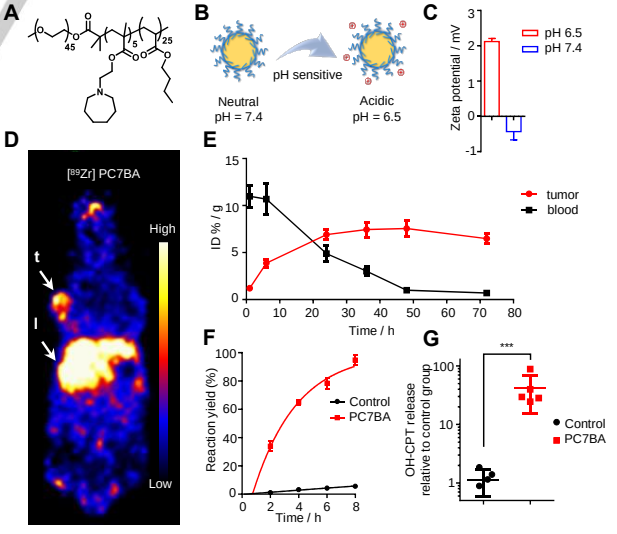

Figure 6. A pH-sensitive polymeric micelle used as a catalyst for Phe-BF_3-mediated desilylation. (**A**) Chemical structure of PEO_{45}-*b*-$PC7A_5$-*b*-PBA_{25} (PC7BA) polymers. (**B**) Schematic representation of pH-responsive working principle of PC7BA micelles. (**C**) Zeta potential of PC7BA micelles in a buffer of pH = 7.4 (blue bar) and 6.5 (red bar). (**D**) PET imaging of [^{89}Zr]PC7BA micelles in BGC823-tumor bearing mouse at 36-hour time point after tail-vain injection. t, tumor; l, liver. (**E**) Time-activity curve of [^{89}Zr]PC7BA micelle in blood and tumor in BGC823 tumor–bearing mice. (**F**) Time-"decaging" yield curve of TBDPSO-CPT+Phe-BF_3 reaction treated by 1 mg/mL PC7BA micelles or 1 mg/mL $PLGA_{5k}$-PEG_{2k} (as negative control) micelles at pH = 6.5. (**G**)

Quantitative analysis of OH-CPT released in tumors in mice treated by PC7BA micelles–delivered TBDPSO-CPT+Phe-BF_3 and $PLGA_{5k}$-PEG_{2k} micelles–delivered TBDPSO-CPT+Phe-BF_3, respectively.

In this work, we take DOTAP and PC7BA micelle as the examples to show that the cationic micelles may function as the catalyst to remarkably accelerate the desilylation reaction both *in vitro* and *in vivo*. According to the mechanistic study, this catalytic nature should be applicable for all cationic micelles as well as the pH-sensitive micelles. Therefore, micelle-catalyzed desilylation offers an exciting opportunity to tissue-selectively activate prodrugs without intrinsic tissue-targeting. In addition, inspired by the fact that many reactions are remarkably faster in organic solvent or micelles than in water, we expect that micelles would be versatile to catalyze a broad scope of reactions *in vivo*.

Acknowledgment

This work was financially supported by National Natural Science Foundation of China (no. NSFC U1867209 and no. NSFC 21778003) and the Ministry of Science and Technology of the Peoples Republic of China (2017YFA0506300).

Keywords: Micellar catalysis, desilylation, controlled release, *in vivo* chemistry

[1] a) J. A. Prescher, C. R. Bertozzi, *Nat. Chem. Biol.* **2005**, *1*, 13-21; b) V. Kenward, T. Katsunori, in *Handbook of In Vivo Chemistry in Mice*, **2020**, pp. 309-353; c) Y. Zheng, X. Ji, B. Yu, K. Ji, D. Gallo, E. Csizmadia, M. Zhu, M. R. Choudhury, L. K. C. De La Cruz, V. Chittavong, Z. Pan, Z. Yuan, L. E. Otterbein, B. Wang, *Nat. Chem.* **2018**, *10*, 787-794; d) R. Rossin, R. M. Versteegen, J. Wu, A. Khasanov, H. J. Wessels, E. J. Steenbergen, W. Ten Hoeve, H. M. Janssen, A. van Onzen, P. J. Hudson, M. S. Robillard, *Nat. Commun.* **2018**, *9*, 1484.

[2] a) L. P. Hammett, *Physical organic chemistry; reaction rates, equilibria, and mechanisms*, 1st ed. ed., McGraw-Hill Book Company, Inc., New York and London, **1940**; b) J. Wang, X. Wang, X. Fan, P. R. Chen, *ACS Cent. Sci.* **2021**.

[3] J. Li, P. R. Chen, *Nat. Chem. Biol.* **2016**, *12*, 129-137.

[4] a) J. Tu, M. Xu, S. Parvez, R. T. Peterson, R. M. Franzini, *J. Am. Chem. Soc.* **2018**, *140*, 8410-8414; b) J. Kim, C. R. Bertozzi, *Angew. Chem., Int. Ed. Engl.* **2015**, *54*, 15777-15781; c) R. M. Versteegen, R. Rossin, W. ten Hoeve, H. M. Janssen, M. S. Robillard, *Angew. Chem., Int. Ed. Engl.* **2013**, *52*, 14112-14116; d) Q. Fu, H. Li, D. Duan, C. Wang, S. Shen, H. Ma, Z. Liu, *Angew. Chem., Int. Ed. Engl.* **2020**, *59*, 21546-21552; e) M. Jiang, H. Li, H. Yang, H. Fu, *Angew. Chem., Int. Ed. Engl.* **2017**, *56*, 874-879; f) Y. Li, Z. Lou, H. Li, H. Yang, Y. Zhao, H. Fu, *Angew. Chem., Int. Ed. Engl.* **2020**, *59*, 3671-3677.

[5] Q. Wang, Y. Wang, J. Ding, C. Wang, X. Zhou, W. Gao, H. Huang, F. Shao, Z. Liu, *Nature* **2020**, *579*, 421-426.

[6] L. Su, R. Li, S. Khan, R. Clanton, F. Zhang, Y. N. Lin, Y. Song, H. Wang, J. Fan, S. Hernandez, A. S. Butters, G. Akabani, R. MacLoughlin, J. Smolen, K. L. Wooley, *J. Am. Chem. Soc.* **2018**, *140*, 1438-1446.

[7] M. A. Mintzer, E. E. Simanek, *Chem. Rev.* **2009**, *109*, 259-302.

[8] S. Yang, Q. Tang, L. Chen, J. Chang, T. Jiang, J. Zhao, M. Wang, P. R. Chen, *Angew. Chem., Int. Ed. Engl.* **2020**, *59*, 18087-18094.

[9] a) S. Du, S. S. Liew, L. Li, S. Q. Yao, *J. Am. Chem. Soc.* **2018**, *140*, 15986-15996; b) M. Zhang, C. C. Song, F. S. Du, Z. C. Li, *ACS Appl. Mater. Interfaces* **2017**, *9*, 25905-25914; c) S. Su, Y. Y. Wang, F. S. Du, H. Lu, Z. C. Li, *Adv Funct Mater* **2018**, *28*, 1805287.

[10] Q. Cheng, T. Wei, L. Farbiak, L. T. Johnson, S. A. Dilliard, D. J. Siegwart, *Nat. Nanotechnol.* **2020**, *15*, 313-320.

[11] a) H. Cabral, K. Miyata, K. Osada, K. Kataoka, *Chem. Rev.* **2018**, *118*, 6844-6892; b) K. Ulbrich, K. Hola, V. Subr, A. Bakandritsos, J. Tucek, R. Zboril, *Chem. Rev.* **2016**, *116*, 5338-5431.

[12] a) B. H. Lipshutz, S. Ghorai, A. R. Abela, R. Moser, T. Nishikata, C. Duplais, A. Krasovskiy, R. D. Gaston, R. C. Gadwood, *J. Org. Chem.* **2011**, *76*, 4379-4391; b) S. Klingelhofer, W. Heitz, A. Greiner, S. Oestreich, S. Forster, M. Antonietti, *J. Am. Chem. Soc.* **1997**, *119*, 10116-10120; c) S. Wallace, E. P. Balskus, *Angew. Chem., Int. Ed. Engl.* **2016**, *55*, 6023-6027.

[13] T. Dwars, E. Paetzold, G. Oehme, *Angew. Chem., Int. Ed. Engl.* **2005**, *44*, 7174-7199.

[14] a) Z. Li, Z. Kong, J. Chen, J. Li, N. Li, Z. Yang, Y. Wang, Z. Liu, *Eur. J. Nucl. Med. Mol. Imaging* **2021**; b) Z. Liu, H. Chen, K. Chen, Y. Shao, D. O. Kiesewetter, G. Niu, X. Chen, *Sci. Adv.* **2015**, *1*, e1500694.

[15] T. W. W. Greene, P. G. M. , *John Wiley & Sons: New York* **1991**.

[16] J. Rautio, N. A. Meanwell, L. Di, M. J. Hageman, *Nat. Rev. Drug Discovery* **2018**, *17*, 559-587.

[17] D. Motoda, H. Kinoshita, H. Shinokubo, K. Oshima, *Angew. Chem., Int. Ed. Engl.* **2004**, *43*, 1860-1862.

[18] R. Hu, J. Feng, D. Hu, S. Wang, S. Li, Y. Li, G. Yang, *Angew. Chem., Int. Ed. Engl.* **2010**, *49*, 4915-4918.

[19] a) I. M. Umlong, K. Ismail, *Colloids Surf., A* **2007**, *299*, 8-14; b) N. Scholz, T. Behnke, U. Resch-Genger, *J. Fluoresc.* **2018**, *28*, 465-476; c) S. K. Hait, S. P. Moulik, *J. Surfactants Deterg.* **2001**, *4*, 303-309.

[20] X. Ji, C. Zhou, K. Ji, R. E. Aghoghovbia, Z. Pan, V. Chittavong, B. Ke, B. Wang, *Angew. Chem., Int. Ed. Engl.* **2016**, *55*, 15846-15851.

[21] W. M. Haynes, D. R. Lide, *CRC handbook of chemistry and physics : a ready-reference book of chemical and physical data*, 91st ed. / ed., Boca Raton (Fla.) : CRC Press, **2010**.

[22] W. Hu, L. Zeng, Y. Wang, Z. Liu, X. Ye, C. Li, *Analyst* **2016**, *141*, 5450-5455.

[23] Y. Qi, Y. Huang, B. Li, F. Zeng, S. Wu, *Anal. Chem.* **2018**, *90*, 1014-1020.

[24] D. Duan, H. Liu, Y. Xu, Y. Han, M. Xu, Z. Zhang, Z. Liu, *ACS Appl. Mater. Interfaces* **2018**, *10*, 5278-5286.

[25] M. Yu, J. Zheng, *ACS Nano* **2015**, *9*, 6655-6674.

[26] M. J. Mitchell, M. M. Billingsley, R. M. Haley, M. E. Wechsler, N. A. Peppas, R. Langer, *Nat. Rev. Drug Discov.* **2021**, *20*, 101-124.

[27] a) T. Volk, E. Jahde, H. P. Fortmeyer, K. H. Glusenkamp, M. F. Rajewsky, *Br. J. Cancer* **1993**, *68*, 492-500; b) K. Zhou, Y. Wang, X. Huang, K. Luby-Phelps, B. D. Sumer, J. Gao, *Angew. Chem., Int. Ed. Engl.* **2011**, *50*, 6109-6114; c) J. Z. Du, T. M. Sun, W. J. Song, J. Wu, J. Wang, *Angew. Chem., Int. Ed. Engl.* **2010**, *49*, 3621-3626; d) S. S. Han, Z. Y. Li, J. Y. Zhu, K. Han, Z. Y. Zeng, W. Hong, W. X. Li, H. Z. Jia, Y. Liu, R. X. Zhuo, X. Z. Zhang, *Small* **2015**, *11*, 2543-2554.

10.1002/anie.202106526

WILEY-VCH

RESEARCH ARTICLE

Entry for the Table of Contents

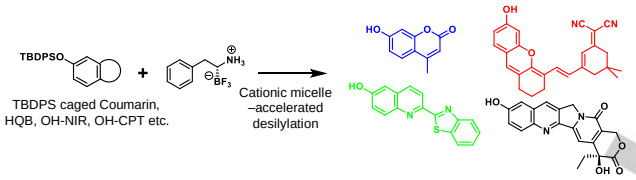

Cationic micelles accelerate desilylation-induced cleavage chemistry over 1400-fold under physiological conditions. This micelle-catalyzed desilylation strategy unveils the potential that micelle may act beyond a carrier but an *in vivo* catalyst for local perturbing or activation.